

Article

Uptake Routes and Biodistribution of Polystyrene Nanoplastics on Zebrafish Larvae and Toxic Effects on Development

Martina Contino ^{1,*}, Greta Ferruggia ¹, Roberta Pecoraro ¹, Elena Maria Scalisi ¹, Gianfranco Cavallaro ², Carmela Bonaccorso ², Cosimo Gianluca Fortuna ², Antonio Salvaggio ³, Fabiano Capparucci ⁴, Teresa Bottari ⁵ and Maria Violetta Brundo ¹

¹ Department of Biological, Geological and Environmental Sciences, University of Catania, Via Androne 81, 95124 Catania, Italy; greta.ferruggia@phd.unict.it (G.F.); roberta.pecoraro@unict.it (R.P.); elenamaria.scalisi@unict.it (E.M.S.); mariavioletta.brundo@unict.it (M.V.B.)

² Department of Chemical Sciences, Viale Andrea Doria 6, 95125 Catania, Italy;

gianfrancocav9234@gmail.com (G.C.); carmela.bonaccorso@unict.it (C.B.); cg.fortuna@unict.it (C.G.F.)

³ Experimental Zooprophyllactic Institute of Sicily “A. Mirri”, Via Gino Marinuzzi, 3, 90129 Palermo, Italy; antonio.salvaggio@izssicilia.it

⁴ Department of Chemical, Biological, Pharmaceutical and Environmental Science, University of Messina, 98166 Messina, Italy; fcapparucci@unime.it

⁵ Institute for Marine Biological Resources and Biotechnology (IRBIM), National Research Country (CNR), 98122 Messina, Italy; teresa.bottari@irbim.cnr.it

* Correspondence: martina.contino@phd.unict.it; Tel.: +39-3271681121

Abstract: Polystyrene (PS) is the most widely used plastic polymer. It is mainly used to produce disposable products. Due to its resistance to degradation, PS can remain in the environment for a long time. Its mechanical, physical and biological actions determine the release of smaller fragments, which are able to penetrate organisms and accumulate in target organs. Fertilized *Danio rerio* eggs were exposed to concentrations of 10 and 20 mg/L of fluorescent, amino-modified polystyrene nanoplastics (nPS-NH₂) with diameters of 100 and 50 nm for 96h, according to OECD guidelines (2013). Uptake, biodistribution, toxicity, oxidative stress and apoptosis were evaluated; moreover, we carried out a simulation to study the interactions between nPS-NH₂ and defined regions of three receptors: STRA6, Adgrg6 and CNTN4/APLP2. We demonstrated that after being internalized, nPS-NH₂ could reach the head and bioaccumulate, especially in the eyes. Moreover, they could lead to oxidative stress and apoptosis in the several regions where they bioaccumulated due to their interaction with receptors. This study confirmed the danger of nanoplastic wastes released in the environment.

Keywords: marine litter; *Danio rerio*; ROS; apoptosis; receptor STRA6; receptor Adgrg6; receptor CNTN4/APLP2



Citation: Contino, M.; Ferruggia, G.; Pecoraro, R.; Scalisi, E.M.; Cavallaro, G.; Bonaccorso, C.; Fortuna, C.G.; Salvaggio, A.; Capparucci, F.; Bottari, T.; et al. Uptake Routes and Biodistribution of Polystyrene Nanoplastics on Zebrafish Larvae and Toxic Effects on Development. *Fishes* **2023**, *8*, 168. <https://doi.org/10.3390/fishes8030168>

Academic Editor: Laura Sánchez

Received: 8 February 2023

Revised: 11 March 2023

Accepted: 17 March 2023

Published: 20 March 2023



Copyright: © 2023 by the authors. Licensee MDPI, Basel, Switzerland. This article is an open access article distributed under the terms and conditions of the Creative Commons Attribution (CC BY) license (<https://creativecommons.org/licenses/by/4.0/>).

1. Introduction

In recent decades, plastic contamination has become a major concern worldwide, as annual plastic production and its application in various fields have increased dramatically [1]. Plastic has now become synonymous with malleability and flexibility, and the products obtained have exceptional characteristics: they are economical, light, durable and resistant to corrosion [2]. One of the main causes of the unstoppable increase in the production of plastic materials, in addition to their chemical–physical characteristics, is dictated by their high shelf life. Consequently, they remain in the environment for a long time as plastic waste. Only 9% of this waste is recycled, while 12% is incinerated and 79% ends up in landfills. Consequently, plastic waste in the environment is fragmented into microparticles with a high index of danger to our health [3].

Through the function of their size, plastic fragments can be classified as microplastics (MPs, dimensions between 0.1 and 5000 µm) and nanoplastics (NPs, dimensions between

1 and 100 nanometers), obtained from the chemical, physical and mechanical degradation of plastic released in the environment [4]. The pollution caused by micro- and nanoplastics is a topic of growing interest; in fact, due to their slow degradation and their small size, these particles can also be ingested by different animal species, causing physiological complications with the possibility of transport in different districts of the organism and along the trophic network, giving rise to bioaccumulation [5].

Plastic debris or marine litter from the early 1970s are already present in the literature [6], but only in recent years has the topic received the growing interest of researchers. Many studies focused on the effects that plastic and its fragments of different sizes could have on aquatic organisms, such as fish and crustaceans, but also on terrestrial organisms, such as birds and mammals [7–9]. The ingestion of plastic material by living organisms represents a risk for the biota; microplastics can cause pathological stress, false satiety, reproductive complications, oxidative stress, block enzyme production and reduce growth rates [10].

Polystyrene is one of the most produced plastics and consequently also one of the most widespread types of plastic debris in the environment [11]. Polystyrene polymers are often chemically modified (with the addition of amino or carboxyl groups) to make them resistant to degradation and for that reason, they are the most widely synthesized for a wide range of applications including biosensors, photonics and nanocomposites [12]. We decided to evaluate the uptake routes and biodistribution of amine-modified polystyrene nanoplastics in zebrafish (*Danio rerio*) embryos, an excellent model for the environmental biomonitoring of aquatic environments [13]. First, we observed the localization of nPS-NH₂ throughout embryonic development at 24h intervals. Following the identification of nPS-NH₂ localization, receptors, which are most prevalent in larvae during embryonic development, were identified based on the structural similarities of ligands to nPS-NH₂, especially in the presence of amino groups. The eventual interaction between each receptor and nPS-NH₂ was reconstructed in silico. This analysis allowed for the identification of the receptor pockets most akin to binding, all possible chemical bonds that could be established (strong or weak) and the binding affinity. In addition, our study aimed to deepen the knowledge already present in the literature, highlighting, for example, the change in nPS-NH₂ localization during embryonic development, evaluating the stimulation of oxidative stress and apoptosis and, as previously mentioned, aiming to identify their possible interactions with the main receptors expressed during embryonic development. In fact, a few studies conducted on zebrafish larvae proved that micro- and nanoplastics could be neurotoxic during development [14] and could cause a decrease in heartbeat, hatching rate, and larvae length [15].

2. Materials and Methods

2.1. Nanoplastics

Autofluorescent, amino-modified polystyrene nanoplastics were purchased from Sigma-Aldrich (Saint Louis, MO, USA). The two types of microspheres were characterized by a density of 1.04–1.06 g/cm³ and a diameter of 100 and 50 nm, respectively. The former presented an orange fluorescence with an excitation/emission wavelength of 481/644 nm, while the latter presented a blue fluorescence and had an excitation/emission wavelength of 358/410 nm. Concentrations suggested by other studies and tested on other animal models, such as *Artemia franciscana* and *Brachionus plicatilis*, were selected [16]. These were higher concentrations than those found in nature, but the purpose of the present work was to investigate the possible uptake of nPS-NH₂ by zebrafish, highlighting possible mechanisms of toxicity resulting from uptake and bioaccumulation. From the stock solution, which consisted of the nPS-NH₂ in an aqueous suspension, working solutions were prepared with concentrations of 10 and 20 mg/L in fresh water.

2.2. Zebrafish Embryo Toxicity Test (ZFET)

The experiment was conducted following OECD guidelines (2013) [17]. Zebrafish embryos were obtained by the Centre for Experimental Fish Pathology of Sicily (CISS) at Department of Veterinary Science of Messina University, Italy. CISS is accredited for the use of aquatic animals in the scientific research (DM n° 39/March/2006). Adults were maintained in a standalone facility (ZebTec, Tecniplast) under controlled conditions (14 h light/10 h dark regimen; temperature 27–28 °C; pH 7.5; conductivity 600 µS/cm). The embryos were placed randomly in 24-well plates within 90 min after fertilization. The negative control (24 eggs) was prepared by exposing the embryos to an embryo medium, while the positive control (20 eggs) was prepared by exposing the embryos to 4 mg/L of 3,4-dichloroaniline, 98% (Acros Organics, The Hague, Belgium). Twenty embryos (one for each well) were exposed to each nanoplastic concentration, while the remaining four wells were used as an internal plate control. All wells were topped up every 24 h with their respective solutions to avoid desiccation (semi-static assay). The embryos were maintained in the tested solutions at a temperature of 26 ± 1 °C (pH 6.5–8.5). The test duration was 96 h, and observations regarding viability and hatching rate were performed every 24 h through a stereomicroscope (Leica EZ4). The following parameters were observed: embryonic mortality, embryonic coagulation, failure to form somites, tail and spinal column deformity and lack of heartbeat. For this experiment, three replicates were performed.

2.3. Localization of Nanoplastics

To determine the localization of nPS-NH₂ and any interactions between them and the organisms, embryos were observed at 24 h intervals under a fluorescence microscope (Nikon eclipse Ci). The images were analyzed using Nis Element software (version 5.20), through which surface intensity plots were obtained. In these plots, the fluorescence intensity was represented by higher or lower peaks. A blue-yellow gradation for 50 nm nPS-NH₂, a green gradation for the 100 nm nPS-NH₂ and a gray scale for the control were selected. Finally, images of 3 larvae per concentration were subjected to an image analysis to determine the differences in the fluorescence intensity (semi-quantitative analysis) of the body areas in which nPS-NH₂ bioaccumulation occurred at 96 h between the exposed and the control groups. Quantification was performed by creating “ROIs” (regions of interest) designed to analyze the same area in all larvae considered [18].

2.4. Cell Apoptosis Analysis

A cell apoptosis analysis was performed using Acridine Orange (AO, Invitrogen, Waltham, MA, USA) [16], a fluorescent dye that interacts with nucleic acids through electrostatic bonds. After a wash in phosphate-buffered saline (PBS, Sigma-Aldrich, Saint Louis, MO, USA), 10 larvae per concentration were incubated with 5 µg/mL AO solution for 20 min at room temperature. The larvae were washed in PBS and observed under a fluorescence microscope (Nikon eclipse Ci). The images were analyzed using the Nis Element (version 5.20) software, which provided the fluorescence intensity. Body parts that showed fluorescence greater than or equal to 40 (values obtained with the control) were considered positive. In addition, fluorescence peaks equal to or greater than 100 were considered more significant. Three replicates were performed.

2.5. Oxidative Stress Analysis

The production of reactive oxygen species (ROS) was examined using the 2',7'-dichlorofluorescein diacetate probe (DCFH₂-DA, Sigma Aldrich, Saint Louis, MO, USA), which emits green fluorescence that is observable with the specific FITC filter when oxidized. The stock solution (130 µM) was diluted in dimethyl sulfoxide (DMSO, Sigma-Aldrich, Saint Louis, MO, USA), divided into individual aliquots and stored at −20 °C. An aliquot was thawed and diluted to a concentration of 5 µM in Hank's Balanced Salt Solution (HBSS, Sigma-Aldrich, Saint Louis, MO, USA) to perform the protocol. Ten larvae were washed in HBSS and incubated with DCFH₂-DA for 15 min at 28 °C in the dark. The larvae

were washed in HBSS and observed under a fluorescence microscope (Nikon eclipse Ci) equipped with a camera (Nikon DS-Qi2). The fluorescence intensity was provided by the Nis Element (version 5.20) software. Body parts showing fluorescence greater than or equal to 40 (a threshold value below which the larvae did not show fluorescence) were considered positive. In addition, fluorescence peaks equal to or greater than 100 were considered more significant. Three replicates were performed.

2.6. Morphological Analysis by Scanning Electron Microscope (SEM)

To detect the morphology of the larvae in detail, a dehydration protocol, which was necessary to observe the organisms under the SEM (Coxem EM-30 plus), was performed. The larvae were fixed in 2.5% glutaraldehyde in PBS for 24 h at 4 °C. Subsequently, the larvae were washed in PBS for 10 min and dehydrated with a series of alcohols of increasing concentration (35°, 50°, 70°, 95° and 100°). The samples were incubated with hexamethyldisylazine (HDMS, Merck, Dramstadt, Germany) and alcohol 100° (1:1 ratio, *v/v*) for 5 min, in pure HDMS for 5 min and left to air dry overnight. The samples were mounted on specific carbon fiber-covered stubs and observed by SEM (Coxem EM-30 plus).

2.7. Structure-Based Virtual Screening

FLAP (Fingerprint for Ligand and Protein) is a software developed at the University of Perugia, in collaboration with Pfizer, and is used for virtual screening as it describes the interactions between small molecules and protein structures. The software detects the interaction fields (MIFs), calculated in GRID, which represent the interactions between the small molecules and the so-called pockets, regions of the protein structure's interaction. In this experiment, the FLAP software was used in the "structure-based" mode to generate binding poses of a ligand in a protein cavity based on the similarity between their GRID fields. The GRID molecular interaction fields were calculated using specific probes, reported in Table S1, to mimic the biological environment. At the end of each screening, the software generates scores (SCORE) that quantify all the ligand–protein interactions; the two fundamental values for a global evaluation of the interactions involved are Glob-Sum-SUM and Glob-Prod, the summation and production of all interactions, respectively.

The amino-modified polystyrene nanoparticle used for the screening was drawn and saved with Chemdraw software (Figure S1). The structure was subsequently transferred to the database created on FLAP, and screenings were finally made on three protein targets.

The crystallized protein targets screened were receptors for retinol uptake *stra6* (STRA6); Adhesion G protein–coupled receptor G6 (*Adgrg6*; also named GPR126), contactin 4 (CNTN4) and amyloid beta precursor-like protein 2 (APLP2) complex (Figure S2). These receptors, mainly expressed in the nervous system, were selected based on the localization of the nPS-NH₂ during embryonic development and the structural similarity of their respective ligands with nPS-NH₂, mainly due to the presence of amino groups. As these receptors are mainly expressed in circuits of the nervous system, the analysis evaluated the possible neurotoxicity of the nPS-NH₂.

2.8. Statistical Analysis

A statistical analysis was performed using *Prism 9*. Differences between the control and exposed groups were assessed by an ANOVA, followed by an ad hoc test (Tukey's test) for intragroup differences. The statistical significance was set at alpha < 0.05 and is indicated by the symbol *. All data are represented as mean ± standard deviation.

3. Results

3.1. Uptake and Biodistribution of Nanoplastics in Zebrafish Larvae

During the 96 hpf of exposure to fluorescent, amino-modified nPS-NH₂ of 100 nm (green) and 50 nm (blue), internalization was observed exclusively for blue nPS-NH₂ into zebrafish larvae before hatching (Figure 1A); after hatching, green nPS-NH₂ were also internalized. After penetration, NPs reached the head and bioaccumulated, especially

in the eyes and in the yolk sac. The uptake of nPS-NH₂ occurred through the yolk sac, which determined distribution of nPS-NH₂ in the rest of the body. Figure 1B shows the trend of nPS-NH₂ localization through fluorescence peaks during the zebrafish embryonic development on exposed organisms compared to the control. The 50 nm nPS-NH₂ at a concentration of 10 mg/L and at 24 hpf showed the highest fluorescence intensity (green/yellow), localized at the level of the embryo. In addition, a fluorescence spot had extended from the chorion to the embryo. This spot likely identified the entry point of the nPS-NH₂ absorbed into the sac from the chorion by the embryo. At 48 hpf, positivity corresponded mainly to the yolk sac and the anterior part of the head, which showed yellow peaks. In addition, spikes were present all over the chorion. These corresponded to new particles, given that our experiment was semi-static, and wells were topped up every 24 hpf. At 72 hpf, a decrease in fluorescence in the yolk sac and an increase in the anterior part of the head were observed. In addition, several peaks were found in the tail. At 96 hpf, a slight diffuse fluorescence throughout the embryo and elevated peaks, corresponding to the yolk sac and eye, were noted. This trend was observed in $88\% \pm 0.04$ ($p < 0.01$ **) of the larvae. As expected, at the concentration of 20 mg/L, the 50 nm nPS-NH₂, showed the same uptake as the lower concentration (10 mg/L), but the fluorescence peaks were higher. At 24 hpf, nPS-NH₂ were already absorbed by the embryo. In addition, many peaks were localized leaning against the chorion. At 48 hpf, the greatest fluorescence was found at the yolk sac and in the anterior part of the body. At 72 hpf, yolk sac and head positivity were also joined by tail positivity. Finally, at 96 hpf, diffuse fluorescence throughout the organisms and high peaks at the levels of the eyes, head and yolk were observed. This positivity was regarded in $90\% \pm 0.03$ ($p < 0.01$ **) of larvae. Concerning the nPS-NH₂ with a diameter of 100 nm (10 mg/L) and up to 72 hpf, peaks were located on the chorion, while the embryo was negative. At 96 hpf, the presence of nPS-NH₂ was identified only in the eye. Of the larvae, $93\% \pm 0.03$ ($p < 0.01$ **) demonstrated this biodistribution of nanoplastics. The trend of major concentration matched that of the lower-diameter nPS-NH₂ and concerned $95\% \pm 0.01$ ($p < 0.01$ **) of the tested organisms. Up to 72 hpf, as time passed, there was an increase in nPS-NH₂ leaning in the chorion, while at 96 h, the fluorescence was localized mainly at the yolk sac level and in the eye. All organisms in the control group remained negative for all 96 h.

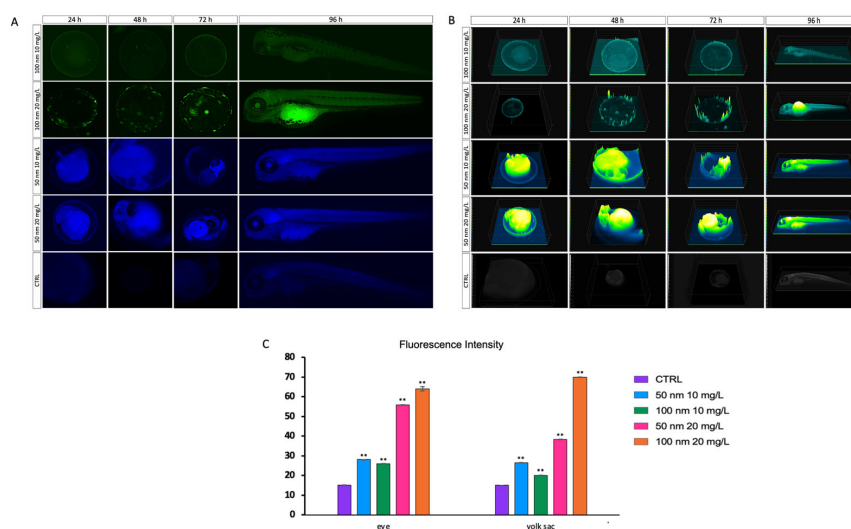


Figure 1. (A) Accumulation and biodistribution of PS-NPs (50 and 100 nm) at different concentrations in *D. rerio* embryos and larvae. The observations were carried out in 24 h intervals; (B) surface fluorescence intensity plot obtained by analyzing the images of biodistribution of PS-NPs (50 and 100 nm) at different concentrations in *D. rerio* embryos and larvae; (C) fluorescence intensity calculated on the ROIs considered (eye and yolk sac) at 96 hpf. Strong statistical differences were found between control groups and all organisms exposed ($p < 0.01$ **).

An image analysis performed on the eyes and yolk of the larvae at 96 hpf showed higher fluorescence intensity in the yolk sac for higher concentrations of both nanoplastics (38.29 ± 0.01 for nPS-NH₂ of 50 nm and 69.98 ± 0.04 for nPS-NH₂ 100 nm) than the lower concentration (26.58 ± 0.03 for nPS-NH₂ of 50 nm and 20.06 ± 0.02 for nPS-NH₂ 100 nm). The same trend occurred for the eyes. The fluorescence intensity increased with the increasing tested concentration (50 nm: 28.01 ± 0.04 for 10 mg/L and 55.73 ± 0.03 for 20 mg/L; 100 nm: 25.98 ± 0.03 for 10 mg/L and 64.36 ± 0.05 for 20 mg/L). In contrast, the control was negative (15.06 ± 0.04 for eye and 15.05 ± 0.01 for yolk sac) (Figure 1C).

3.2. Survival, Hatch, and Development

Exposure to nPS-NH₂ had no statistically significant impact on the mortality rate of zebrafish larvae (Figure 2A), but had a negative influence on the hatching rate (Figure 2B). Compared to the control, which had a hatching rate of 82%, hatching rates in organisms exposed to 10 mg/L of the two nPS-NH₂ (50 and 100 nm) were found at 11% and 30%, respectively. At higher concentrations, on the other hand, the percentages dropped to 0. In addition, sub-lethal effects were found in almost 7% of the nPS-NH₂-exposed zebrafish larvae at 96 hpf compared to the control group (0%) (Figure 2C). Body malformation, column curvature, lack of tail development and blood pooling were observed in the *D. rerio* larvae exposed to 20 mg/L 50 nm nPS-NH₂ (Figures 3 and 4).

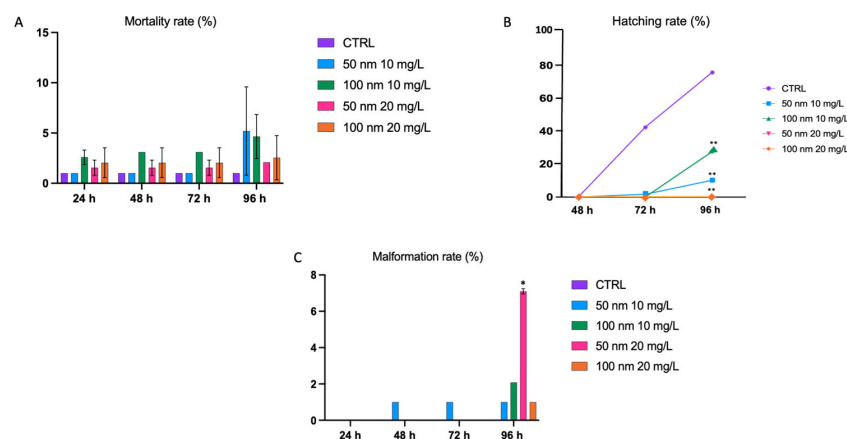


Figure 2. (A) Mortality rate of *D. rerio* embryos exposed to 50 and 100 nm nPS-NH₂ at different concentrations compared to the control group. No statistical differences were found ($p > 0.05$). (B) Hatching rate of *D. rerio* larvae exposed to 50 and 100 nm of nPS-NH₂ at different concentrations compared to the control group. Strong statistical differences were found between control groups and all organisms exposed ($p < 0.01$ **). (C) Malformation rate of *D. rerio* larvae exposed to 50 and 100 nm nPS-NH₂ at different concentrations compared to the control group. The symbol * indicates statistical significance ($p < 0.05$).

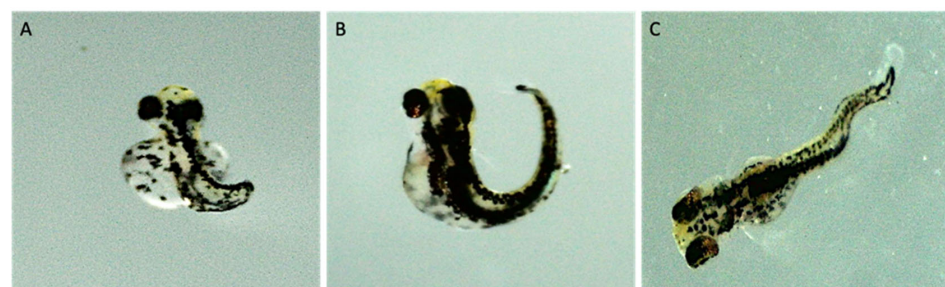


Figure 3. Anomalies observation of *D. rerio* larvae exposed to 20 mg/L 50 nm nPS-NH₂ under a stereomicroscope. (A) Malformation of entire body and lack development of the tail; (B,C) curvature of the tail.

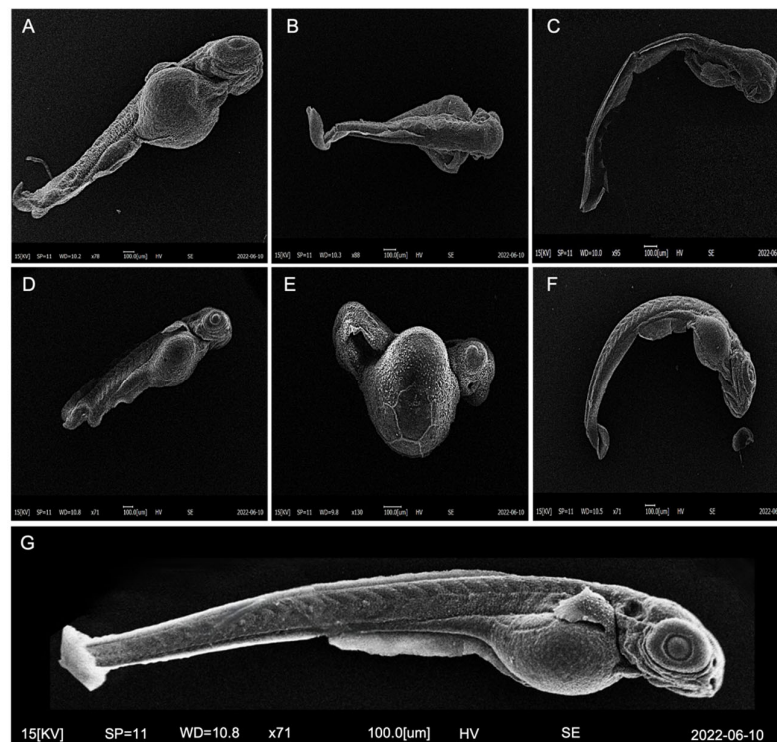


Figure 4. Anomalies observation of *D. rerio* larvae exposed to 20 mg/L 50 nm nPS-NH₂ by SEM. (A,D) Lack development of the tail; (B,E) malformation of entire body; (C,F) curvature of the tail; (G) normal development of the body (control).

3.3. Cell Apoptosis

At the end of the exposure time (96 hpf), cell apoptosis was assessed using the fluorescent dye AO. The fluorescence intensity and its localization are shown in the graphs in Figure 5. Almost all exposed organisms (10 embryos per concentration) were positive compared to the control group. While only 1% of the organisms in the control group showed the presence of some apoptotic cell spots, 54% and 74% of the organisms were positive when exposed to 10 mg/L concentrations of the 50 nm and 100 nm nPS-NH₂, respectively. The number of positive larvae increased with increasing concentrations (75% and 88% for organisms exposed to 20 mg/L of 50 nm and 100 nm nPS-NH₂, respectively) (Figure 6). The fluorescence was mainly localized at the level of the anterior part of the head in the organisms exposed to nPS-NH₂ with a diameter of 100 nm at a concentration of 10 mg/L. At a concentration of 20 mg/L of the same nPS-NH₂, the fluorescence, in addition to peaking at the anterior part of the body, was diffuse throughout the larvae. In larvae exposed to the nPS-NH₂ with a smaller diameter (50 nm), fluorescence was diffuse throughout the larva for both concentrations, with a greater peak at the anterior part of the head. However, at the highest concentration (20 mg/L), the intensity peak was clearly higher than the lowest concentration. In addition, at the highest concentrations of both diameters of nPS-NH₂, spots of apoptotic cells were also identified on the back of the head.

3.4. Oxidative Stress

ROS production and the occurrence of oxidative stress were assessed by exposure of larvae to the fluorescent probe DCFH2-DA. As shown in Figures 7 and 8, larvae exposed to the lowest concentrations (10 mg/L) of both nPS-NH₂ did not exhibit fluorescence (3% for the control, 3% and 4% for larvae exposed to 50 nm and 100 nm nPS-NH₂, respectively), while at the highest concentration, the larvae were positive. Higher peaks were found in larvae exposed to the nPS-NH₂ with a size of 100 nm (97% of positive larvae). Specifically, in larvae exposed to the 100 nm nPS-NH₂, ROS production was localized throughout the larva, with a high peak at the tail termination, followed by a lower peak at the head. For

the 50 nm nPS-NH₂, the highest peak was found at the level of the head, followed by a lower peak at the level of the initial part of the tail (93% of positive larvae).

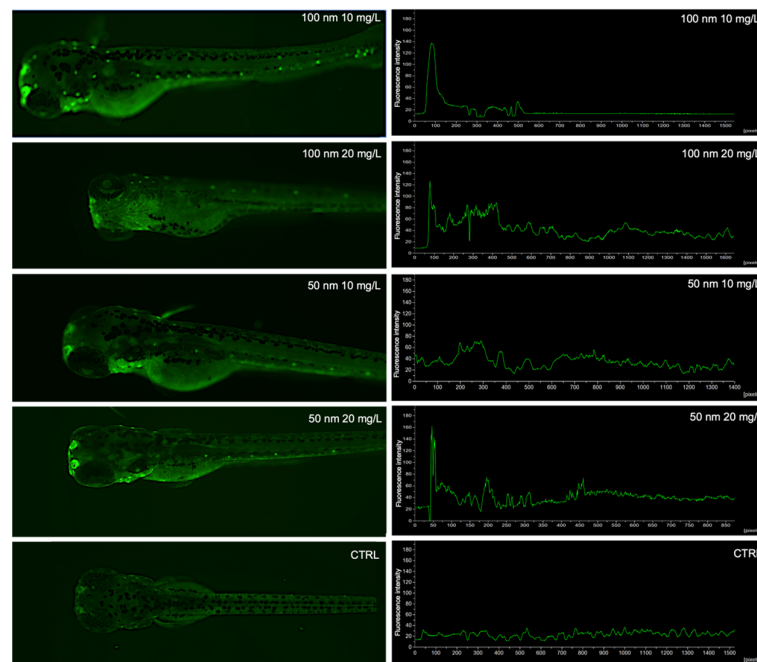


Figure 5. Localization of apoptotic cells on *D. rerio* larvae exposed to nPS-NH₂ and on control. The graphs show the fluorescence intensity, the peaks of which correspond to cells in active apoptosis.

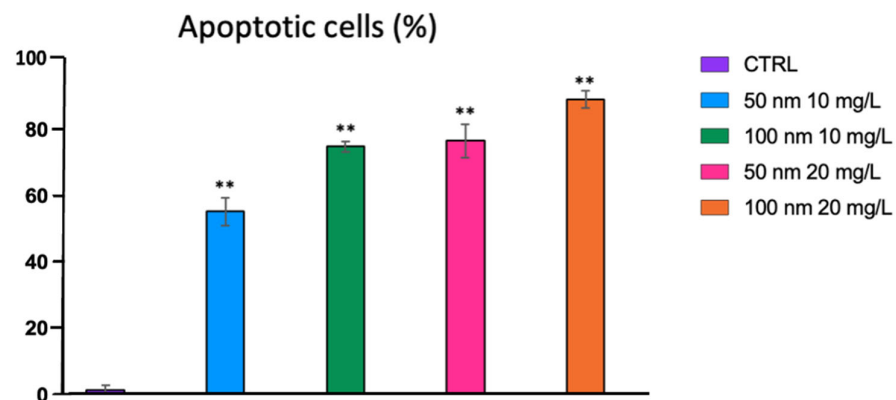


Figure 6. Percentage of organisms exposed to nPS-NH₂ positive for AO compared to the control group. The symbol ** indicates strong statistical significance ($p < 0.01$).

3.5. Virtual Screening

All pockets of the three selected receptors are shown in Figure S3. Table S3 shows all values obtained for the corresponding interactions.

3.5.1. Receptor for Retinol Uptake Stra6 (STRA6)

For the STRA6 receptor, two pockets that were symmetrical and almost overlapping were identified.

Pockets 1 and 2 showed similar bonds, which were not very large, and surfaces. The areas of interaction were minimal, as can be seen in the 2D representations. Specifically, there were only areas of a hydrophobic character distributed in an ununiform way and small donor–acceptor hydrogen bond regions, but these were involved very little in the interaction with the nPS-NH₂. The large difference between the two pockets was the affinities of character π - π and CH- π with the amino acid residues. In fact, an amino acid

residue was observed in the case of Pocket 1, while for Pocket 2, three interactions with the ring aromatic flavor of nPS-NH₂ were highlighted.

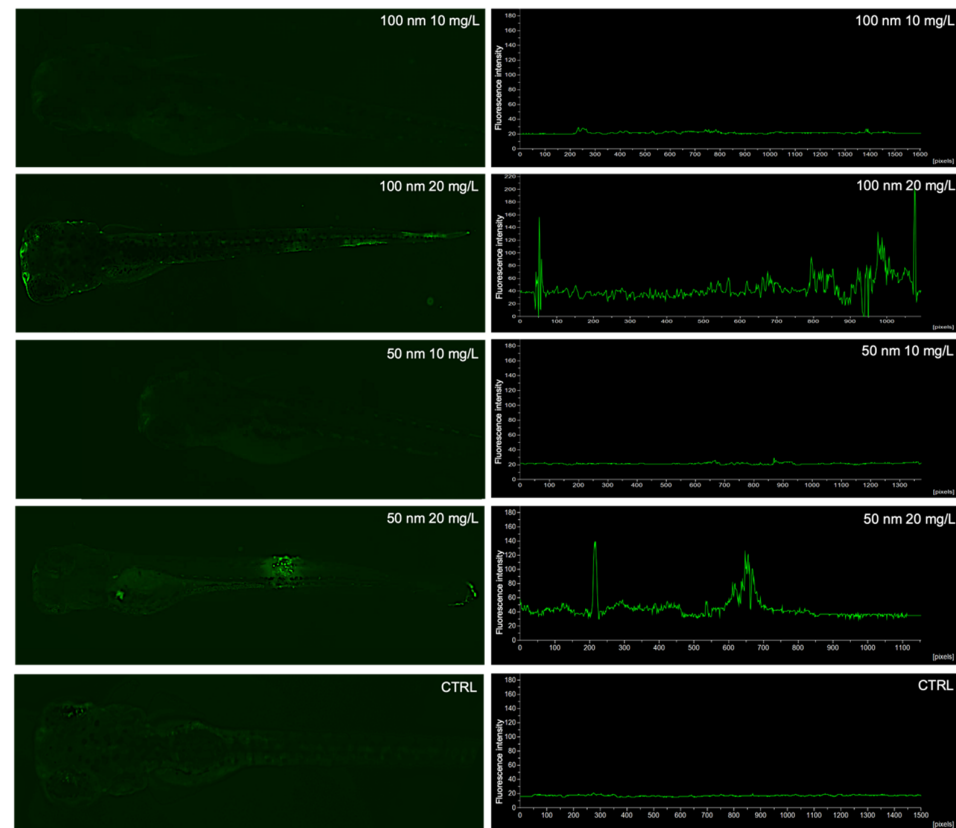


Figure 7. Localization of oxidative stress on *D. rerio* larvae exposed to nPS-NH₂ and in the control group. Fluorescence peaks indicate the presence of ROS.

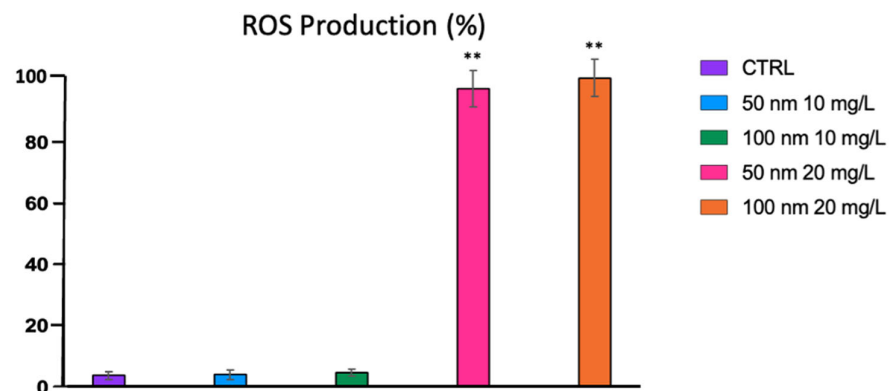


Figure 8. Percentage of organisms exposed to nPS-NH₂ positive for ROS production compared to the control group. Statistical differences ** were observed between control group and organisms exposed to the higher concentration of both nanoplastics ($p < 0.01$).

3.5.2. Adhesion G Protein–Coupled Receptor G6 (Adgrg6 or GPR126)

Five pockets of interest were identified for this receptor. The two largest pockets were 2 and 3, at the top and in the center of the protein target, respectively, and Pockets 1, 4 and 5, at the bottom right, top right and bottom left, respectively. There was no interaction with Pocket 4 (scores close to 0). Pockets 1 and 3 showed higher interaction values, while 2 and 5 were decidedly lower.

Dimensionally, the two pockets had large differences. In fact, while Pocket 1 had reduced dimensions, the size of Pocket 3 was considerably larger. This can be seen both in

the surface of the two pockets and in the binding area. The interaction scores were higher than the other two pockets, as shown in the Glob-Sum values. Pocket 3 had a higher value of N1 than Pocket 1. Regarding the areas of the pocket affected by the supramolecular bonds, there were greater regions of a hydrophobic character (green) for Pocket 1 and, instead, greater acceptor regions of hydrogen bonds (blue) in Pocket 3. In both pockets, the amino group of nPS-NH₂ was involved in the ligand–protein interactions: for Pocket 1, only one aa was involved in the π - π and CH- π bonds, while two aas were involved for Pocket 3.

Pockets 2 and 5 had lower score values than the two previous pockets. This aspect was emphasized by the Glob-Sum of both; the latter had lower values since the N1 and DRY, or bond donor, were lowered, i.e., hydrogen, and the hydrophobic interaction. The value that did not differ between the two previous pockets was H. This denoted a certain compatibility of shape between the pockets and the ligand; in the case of our screenings, the repetitive unit of nPS-NH₂. In both cases, the amino group was involved and interacted, in both pockets, with an aa. This result could be very interesting for the purposes of this research, given that the amino group was the functional group that characterized the surface of the nanoparticle under examination. In fact, although Pockets 2 and 5 had lower Glob-Sum values compared to Pockets 1 and 3 and therefore little interaction on the card, they seemed, at the same time, to involve the amino group more in the interaction phase. Finally, Pocket 4 had interaction values close to zero; it was therefore not possible to predict any type of pose and ligand–protein interaction.

3.5.3. Contactin 4 (CNTN4) and Amyloid Beta Precursor-like Protein 2 (APLP2) Complex

Three pockets of interest were identified for this receptor. Only Pockets 1 and 3 were evaluated, since they showed a Glob-Sum value other than zero. Specifically, the two Pockets, 1 and 3, were very similar to each other, and almost overlapped. In fact, they shared a small area and had almost comparable dimensions. Pocket 2 was in a more secluded position on the right and had a much smaller area than the other two.

From a dimensional point of view, the two pockets were very similar to each other, both in the 2D and 3D representations. In addition, the hydrogen bond and acceptor–donor areas, red and blue, respectively, were comparable, even if they involved the amino group of nPS-NH₂ more in Pocket 1. The green areas were reduced in both pockets, while for the amino acid residues that were more involved in the supramolecular, π - π and CH- π bonds, there was a small difference, i.e., in the case of Pocket 1, four aas were involved without an interaction with the amino group, and there was only one aa in the case of Pocket 3. Similarities were noted also for the Glob-Sum values, with a higher value for Pocket 1. For Pocket 2, we did not report any type of representation since all the interaction values (SCOREs) were close to zero.

Pockets 2 and 5 were also of different sizes. Pocket 2 was decidedly larger than 5. Their scores had lower values than Pocket 1 and 3, and this was emphasized significantly by their Glob-Sum values. The latter had lower values since the N1 and DRY were lowered, i.e., the hydrogen bond donor and hydrophobic interaction. The value that did not differ from the two previous pockets was H: this denoted a certain shape compatibility between the pockets and the ligand. In the case of our screenings, this was the repetitive unit of the nPS-NH₂. In both cases, the amino group was mainly involved and interacted, in both pockets, with an aa. This could be very interesting for the purposes of our study, since it was the amino group that characterized the surface of the tested nanoplastic; in fact, although Pockets 2 and 5 had lower Glob-Sum values compared to Pocket 1 and 3 and therefore little interaction on the card, at the same time, they seemed to involve the amino group more in the interaction phase. Finally, Pocket 4 had interaction values close to zero; and it was therefore not possible to predict any type of pose and ligand–protein interaction.

4. Discussion

The environmental diffusion of nPS-NH₂ requires investigation to clarify possible consequences for living organisms, especially regarding embryonic development, which is more sensitive to the presence of pollutants. The aim of the present experiment was to assess the effects of amino-modified PS-NPs with diameters of 100 nm and 50 nm at different concentrations (10 e 20 mg/L) on the early stages of *Danio rerio* for 96 h. The *in vivo* approach was complemented by an *in silico* analysis to evaluate the ability of nPS-NH₂ to bind specific receptors, acting as an endocrine disruptor.

The *in vivo* analysis focused on multiple endpoints, such as the localization of nPS-NH₂, the hatching rate, viability and occurrence of malformations. The results obtained revealed the transition of the 50 nm nPS-NH₂ from the chorion and absorption by the embryo already from 24 hpf. Instead, the nPS-NH₂ with a larger diameter (100 nm) were captured by the larvae after hatching. The chorion represents a barrier to external substances; however, at the same time, it allows for the exchange of gases and nutrients due to the presence of pores with a diameter of 500–700 nm [16,18]. Although the canals are larger than the diameter of the particles tested, only the 50 nm nPS-NH₂ were absorbed, while the larger nPS-NH₂ leaned against the chorion, as also observed by Duan et al. (2020) [19]. The mechanisms behind selectivity and permeability remain poorly understood.

In the present study, the passage of the 50 nm nPS-NH₂ from the extra-embryonic fluid, filling the perivitelline space to the yolk sac, was also demonstrated. At 24 hpf of exposure, in fact, these nPS-NH₂ were mainly found in the yolk sac, while at 48 h hpf and until 96 hpf, biodistribution caused their accumulation in the anterior part of the body, especially in the head and eyes. The yolk sac is known to contain the nutrients to support the growth of the embryo until it acquires the ability to feed itself and introduce food from the aquatic environment [20]. The mechanism of nPS-NH₂ uptake is unclear, but from studies on other nanoparticles, it could be determined by the activation of specific receptors in the yolk sac epithelium, implicated in the processes of endocytosis or pinocytosis [21]. The yolk sac, containing a large amount of lipids, appears to be the main organ for the accumulation of nPS-NH₂. Interestingly, their affinity towards lipid molecules is known in the literature; thus, an influence of their metabolism is hypothesized [22]. Cholesterol (40%), phosphatidylcholine (17%) and triglycerides (9%), the principal molecules contained in the yolk sac, are the metabolic substrates that produce ATP, which is essential for proper development [23]. This could explain the malformations detected in the embryos exposed to these nPS-NH₂. When contact with the organisms occurred during the early stages of development, the penetration of the 50 nm nPS-NH₂ resulted mainly in tail abnormalities (curved or undeveloped). Such anomalies were not found for the 100 nm nPS-NH₂, which were absorbed after hatching. In fact, accumulation of the 100 nm nPS-NH₂ in the yolk sac and their subsequent biodistribution occurred at 96 hpf, when the larvae were hatched. It is known that from days 4–5 postfertilization, the larvae begin to internalize food from outside [24]. The accumulation of nPS-NH₂ in the yolk was therefore mainly caused by oral exposure. However, some studies suggested that endocytosis mechanisms, typical of the yolk sac epithelium, are still active after hatching. Moreover, absorption through the skin was also documented [25]. Again, however, the yolk was the primary organ of bioaccumulation. This result is in agreement with other studies that initially observed the deposition of almost all the xenobiotics tested at the yolk level and how their quantity decreased in relation to increased biodistribution in other parts of the body until a steady state was reached [24].

Our results showed that nPS-NH₂ did not have lethal effects but did have sub-lethal effects. For example, both nPS-NH₂ caused a delay in hatching in a dose-dependent manner such that at higher concentrations, the hatching rate was ~1%. It is hypothesized that 50 nm nPS-NH₂, absorbed in the perivitelline space, could cause hypoxia and delay hatching. At the same time, the results suggested that 100 nm nPS-NH₂ could also lead to the same effect but with a different mechanism. The formation of aggregates clinging to the chorion could occlude the pores and consequently block gas and nutrient exchanges [19]. In

addition to the identification of abnormalities and delayed hatching, other sub-lethal effects were analyzed by enzymatic assays to elucidate the contribution of nPS-NH₂ to oxidative stress and programmed cell death. By means of Acridine Orange staining, apoptosis was identified throughout the body, especially at the level of the nasal dimples in all exposed larvae. In zebrafish, the olfactory organ represents the main route of interaction with the aquatic environment. Death of or damage to the olfactory epithelium due to contact with contaminants is an indication of neurotoxicity, as it can diminish the ability to perceive odors, which frequently direct the behavior of the animals. It was shown that high levels of apoptosis in nasal dimples are correlated with changes in swimming behavior [26].

The DFCH₂-DA probe allowed for the assessment of oxidative stress, identified mainly at the level of the tail and head in organisms exposed to the highest concentrations of both nPS-NH₂. Although ROS are involved in the stimulation of different metabolic pathways, their imbalance with antioxidant systems increases lipid peroxidation phenomena on major macromolecules (DNA, lipids and proteins) and inflammatory responses [27]. Qiang and Cheng (2019) also reported the mediation of ROS in the activation of apoptosis by the p53 protein in embryos exposed to nanoplastics. The presence of oxidative stress at the head may, therefore, be further linked with the neurotoxicity of nPS-NH₂ [28].

Following the identification of the final location of the PS-NH₂, an *in silico* approach was adopted in this study to assess the potential activity of the tested nanoplastics as endocrine disruptors. They mimic the action of hormones by activating or repressing specific receptors at inappropriate times, causing developmental abnormalities [29]. Using FLAP software, the structures of the candidates were recreated: STRA6, GPR126 and CNTN4/APLP2. The choice of receptors was derived from the accumulation of nPS-NH₂ in zebrafish eyes, highlighted in the present study and confirmed by other authors [30]. For this reason, the potential toxicity in the visual system and the nervous system in general was analyzed. STRA6 is the receptor for retinol (vitamin A), mainly located in the retinal pigment epithelium. Retinol uptake is essential for the proper development and survival of photoreceptors and, consequently, for vision [31]. The GPR126 receptor is abundantly expressed in the peripheral nervous system of vertebrates and is involved in Schwann cell maturation and myelination [32]. The third receptor chosen was CNTN4/APLP2. Contactins are involved in neural cell adhesion and guide the formation and differentiation of neural circuits. In particular, the CNTN4 complex and the amyloid precursor APLP2 stimulate the development of the visual system [33]. The results indicated a higher affinity of nPS-NH₂ for GPR126 receptor Pocket 1 (Glob-Sum: 1831), followed by STRA6 receptor Pocket 2 (Glob-Sum: 1704) and, finally, CNTN4/APLP2 receptor Pocket 1 (Glob-Sum: 1364). These experimental data deepen the knowledge of the neurotoxicity of nPS-NH₂, which was previously investigated by other studies that demonstrated changes in swimming and eating behaviors [34] but did not identify the mechanisms responsible for these consequences. Hence, the ability of polystyrene to bind to these receptors may be responsible for abnormalities in the nervous system, especially in vision.

5. Conclusions

We demonstrated that 100 and 50 nm diameter NPs, after being internalized, can reach the head and bioaccumulate, especially in the eyes. Moreover, they can lead to oxidative stress and apoptosis in the several regions in which they bioaccumulate. We also detected many developmental malformations, confirming the danger of nanoplastic wastes released in the environment.

Supplementary Materials: The following supporting information can be downloaded at: <https://www.mdpi.com/article/10.3390/fishes8030168/s1>, Table S1: In FLAP, the pharmacophores for a ligand are defined in terms of the types of atoms that can interact with the receptor. The types of atoms are classified based on the interactions; Figure S1: The amino-modified polystyrene nanoparticle used for the screening (Chemdraw software). Figure S2: Crystallized structure of receptors. (A) Receptor for retinol uptake stra6 (STRA6); (B) adhesion G protein-coupled receptor G6 (Adgrg6; also named GPR126); (C) contactin 4 (CNTN4) and amyloid beta precursor-like protein 2 (APLP2) complex. Table

S2: Summarized table of all tested parameters, expressed as mean \pm standard deviation. ** indicates statistically significant differences ($p < 0.05$). Figure S3: Crystallized structure of *D. rerio* receptors with visible Pockets. (A) Receptor for retinol uptake stra6 (STRA6) with 2D and 3D visions of Pockets 1 and 2; (B) adhesion G protein-coupled receptor G6 (Adgrg6; also named GPR126) with 2D and 3D visions of Pockets 1, 3, 2 and 5; (C) contactin 4 (CNTN4) and amyloid beta precursor like protein 2 (APLP2) complex with 2D and 3D visions of Pockets 1 and 3. Table S3: Affinity of nPS-NPs toward the pockets of STRA6, GPR126 and CNTN4/APLP2 receptors, based on potential bonding types (summarized through Glob-Sum) and pocket size.

Author Contributions: Conceptualization, M.C. and M.V.B.; methodology, M.C. and G.F.; software, G.C. and C.B.; validation, C.G.F., T.B. and M.V.B.; investigation, M.C., G.F. and F.C.; data curation, M.C. and G.C.; writing—original draft preparation, M.C. and M.V.B.; writing—review and editing, R.P., E.M.S., A.S. and T.B.; supervision, M.V.B.; funding acquisition, M.V.B. All authors have read and agreed to the published version of the manuscript.

Funding: This research received no external funding.

Institutional Review Board Statement: Ethical review and approval were waived for this study since the embryos and larvae used were not developed enough to be protected under national legislation.

Informed Consent Statement: Not applicable.

Data Availability Statement: Original data are available upon request.

Acknowledgments: M.C. thanks funds University of Catania, Italy, MIUR XXXVI cycle PhD.

Conflicts of Interest: The authors declare no conflict of interest.

References

- Shahul Hamid, F.; Bhatti, M.S.; Anuar, N.; Anuar, N.; Mohan, P.; Periathamby, A. Worldwide distribution and abundance of microplastic: How dire is the situation? *Waste Manag. Res.* **2018**, *36*, 873–897. [[CrossRef](#)] [[PubMed](#)]
- Hammer, J.; Kraak, M.H.S.; Parsons, J.R. Plastics in the Marine Environment: The Dark Side of a Modern Gift. In *Reviews of Environmental Contamination and Toxicology*; Whitacre, D., Ed.; Springer: New York, NY, USA, 2012; Volume 220.
- Rosenboom, J.G.; Langer, R.; Traverso, G. Bioplastics for a circular economy. *Nat. Rev. Mater.* **2022**, *7*, 117–137. [[CrossRef](#)]
- Mariano, S.; Tacconi, S.; Fidaleo, M.; Rossi, M.; Dini, L. Micro and Nanoplastics Identification: Classic Methods and Innovative Detection Techniques. *Front Toxicol.* **2021**, *3*, 636640. [[CrossRef](#)] [[PubMed](#)]
- Wright, S.L.; Thompson, R.C.; Galloway, T.S. The physical impacts of microplastics on marine organisms: A review. *Environ. Pollut.* **2013**, *178*, 483–492. [[CrossRef](#)] [[PubMed](#)]
- Carpenter, E.J.; Smith, K.L., Jr. Plastics on the Sargasso sea surface. *Science* **1972**, *175*, 1240–1241. [[CrossRef](#)]
- Carlin, J.; Craig, C.; Little, S.; Donnelly, M.; Fox, D.; Zhai, L.; Walters, L. Microplastic accumulation in the gastrointestinal tracts in birds of prey in central Florida, USA. *Environ. Pollut.* **2020**, *264*, 114633. [[CrossRef](#)]
- Haave, M.; Gomiero, A.; Schönheit, J.; Nilsen, H.; Olsen, A.B. Documentation of Microplastics in Tissues of Wild Coastal Animals. *Front. Environ. Sci.* **2021**, *9*, 575058. [[CrossRef](#)]
- Soe, K.K.; Hajisamae, S.; Sompongchaiyakul, P.; Towatana, P.; Pradit, S. Feeding Habits and the Occurrence of Anthropogenic Debris in the Stomach Content of Marine Fish from Pattani Bay, Gulf of Thailand. *Biology* **2022**, *11*, 331. [[CrossRef](#)] [[PubMed](#)]
- Wang, J.; Li, Y.; Lu, L.; Zheng, M.; Zhang, X.; Tian, H.; Wang, E.; Ru, S. Polystyrene microplastics cause tissue damages, sex-specific reproductive disruption and transgenerational effects in marine medaka (*Oryzias melastigma*). *Environ. Pollut.* **2019**, *254*, 113024. [[CrossRef](#)]
- Lu, Y.; Zhang, Y.; Deng, Y.; Jiang, W.; Zhao, Y.; Geng, J.; Ding, L.; Ren, H. Uptake and Accumulation of Polystyrene Microplastics in Zebrafish (*Danio rerio*) and Toxic Effects in Liver. *Environ. Sci. Technol.* **2016**, *50*, 4054–4060. [[CrossRef](#)]
- Bergami, E.; Pugnolini, S.; Vannuccini, M.L.; Manfra, L.; Faleri, C.; Savorelli, F.; Dawson, K.A.; Corsi, I. Long-term toxicity of surface-charged polystyrene nanoplastics to marine planktonic species *Dunaliella tertiolecta* and *Artemia franciscana*. *Aquat. Toxicol.* **2016**, *189*, 159–169. [[CrossRef](#)]
- Pecoraro, R.; Salvaggio, A.; Marino, F.; Caro, G.D.; Capparucci, F.; Lombardo, B.M.; Messina, G.; Scalisi, E.M.; Tummino, M.; Loreto, F.; et al. Metallic Nano-Composite Toxicity Evaluation by Zebrafish Embryo Toxicity Test with Identification of Specific Exposure Biomarkers. *Curr. Protoc. Toxicol.* **2017**, *74*, 1–14. [[CrossRef](#)]
- Chen, Q.; Gundlaci, M.; Yang, S.; Jiang, J.; Velki, M.; Yin, D.; Hollert, H. Quantitative investigation of the mechanisms of microplastics and nanoplastics toward zebrafish larvae locomotor activity. *Sci. Total Environ.* **2017**, *584–585*, 1022–1031. [[CrossRef](#)]
- Teng, M.; Zhao, X.; Wu, F.; Wang, C.; Wang, C.; White, J.C.; Zhao, W.; Zhou, L.; Yan, S.; Tian, S. Charge-specific adverse effects of polystyrene nanoplastics on zebrafish (*Danio rerio*) development and behavior. *Environ. Int.* **2022**, *163*, 107154. [[CrossRef](#)] [[PubMed](#)]

16. Asharani, P.V.; Wu, Y.L.; Gong, Z.; Valiyaveetil, S. Toxicity of silver nanoparticles in zebrafish models. *Nanotechnology* **2008**, *19*, 255102. [[CrossRef](#)] [[PubMed](#)]
17. OECD. *Test No. 236: Fish Embryo Acute Toxicity (FET) Test, OECD Guidelines for the Testing of Chemicals*; OECD Publishing: Paris, France, 2013.
18. Liu, H.; Nie, F.H.; Lin, H.Y.; Ma, Y.; Ju, X.H.; Chen, J.J.; Gooneratne, R. Developmental toxicity, EROD, and CYP1A mRNA expression in zebrafish embryos exposed to dioxin-like PCB126. *Environ. Toxicol.* **2016**, *31*, 201–210. [[CrossRef](#)]
19. Duan, Z.H.; Duan, X.Y.; Zhao, S.; Wang, X.L.; Wang, J.; Liu, Y.B.; Peng, Y.W.; Gong, Z.Y.; Wang, L. Barrier function of zebrafish embryonic chorions against microplastics and nanoplastics and its impact on embryo development. *J. Hazard. Mater.* **2020**, *395*, 122621. [[CrossRef](#)]
20. Sant, K.E.; Timme-Laragy, A.R. Zebrafish as a Model for Toxicological Perturbation of Yolk and Nutrition in the Early Embryo. *Curr. Environ. Health Rep.* **2018**, *5*, 125–133. [[CrossRef](#)] [[PubMed](#)]
21. Assémat, E.; Chatelet, F.; Chandellier, J.; Commo, F.; Cases, O.; Verroust, P.; Kozyraki, R. Overlapping expression patterns of the multiligand endocytic receptors cubilin and megalin in the CNS, sensory organs and developing epithelia of the rodent embryo. *Gene. Expr. Patterns* **2005**, *6*, 69–78. [[CrossRef](#)] [[PubMed](#)]
22. Rossi, G.; Monticelli, L. Modeling the effect of nano-sized polymer particles on the properties of lipid membranes. *J. Phys. Condens. Matter.* **2014**, *26*, 503101. [[CrossRef](#)]
23. Fraher, D.; Sanigorski, A.; Mellett, N.A.; Meikle, P.J.; Sinclair, A.J.; Gibert, Y. Zebrafish embryonic Lipidomic analysis reveals that the yolk cell is metabolically active in Processing Lipid. *Cell Rep.* **2016**, *14*, 1317–1329. [[CrossRef](#)] [[PubMed](#)]
24. Hernandez, R.F.; Galitan, L.; Cameron, J.; Goodwin, N.; Ramakrishnan, L. Delay of Initial Feeding of Zebrafish Larvae Until 8 Days Postfertilization Has No Impact on Survival or Growth Through the Juvenile Stage. *Zebrafish* **2018**, *15*, 515–518. [[CrossRef](#)]
25. Van Pomeran, M.; Brun, N.R.; Peijnenburg, W.J.G.M.; Vijver, M.G. Exploring uptake and biodistribution of polystyrene (nano)particles in zebrafish embryos at different developmental stages. *Aquat. Toxicol.* **2017**, *190*, 40–45. [[CrossRef](#)] [[PubMed](#)]
26. Calvo-Ochoa, E.; Byrd-Jacobs, C.A. The Olfactory System of Zebrafish as a Model for the Study of Neurotoxicity and Injury: Implications for Neuroplasticity and Disease. *Int. J. Mol. Sci.* **2019**, *20*, 1639. [[CrossRef](#)] [[PubMed](#)]
27. Umamaheswari, S.; Priyadarshinee, S.; Bhattacharjee, M.; Kadirvelu, K.; Ramesh, M. Exposure to polystyrene microplastics induced gene modulated biological responses in zebrafish (*Danio rerio*). *Chemosphere* **2021**, *281*, 128592. [[CrossRef](#)]
28. Qiang, L.Y.; Cheng, J.P. Exposure to microplastics decreases swimming competence in larval zebrafish (*Danio rerio*). *Ecotoxicol. Environ. Saf.* **2019**, *176*, 226–233. [[CrossRef](#)]
29. Monneret, C. What is an endocrine disruptor? *Comptes Rendus Biol.* **2017**, *340*, 403–405. [[CrossRef](#)]
30. Zhang, R.; Wang, M.; Chen, X.; Yang, C.; Wu, L. Combined toxicity of microplastics and cadmium on the zebrafish embryos (*Danio rerio*). *Sci. Total Environ.* **2020**, *743*, 140638. [[CrossRef](#)]
31. Solanki, A.K.; Kondkar, A.A.; Fogerty, J.; Su, Y.; Kim, S.-H.; Lipschutz, J.H.; Nihalani, D.; Perkins, B.D.; Lobo, G.P. A Functional Binding Domain in the Rbpr2 Receptor Is Required for Vitamin A Transport, Ocular Retinoid Homeostasis, and Photoreceptor Cell Survival in Zebrafish. *Cells* **2020**, *9*, 1099. [[CrossRef](#)]
32. Baxendale, S.; Asad, A.; Shahidan, N.O.; Wiggin, G.R.; Whitfield, T.T. The adhesion GPCR Adgrg6 (Gpr126): Insights from the zebrafish model. *Genesis* **2021**, *59*, 23417. [[CrossRef](#)]
33. Karuppan, S.J.; Vogt, A.; Fischer, Z.; Ladutska, A.; Swiastyn, J.; McGraw, H.F.; Bouyain, S. Members of the vertebrate contactin and amyloid precursor protein families interact through a conserved interface. *J. Biol. Chem.* **2022**, *298*, 101541. [[CrossRef](#)] [[PubMed](#)]
34. Manuel, P.; Almeida, M.; Martins, M.; Oliveira, M. Effects of nanoplastics on zebrafish embryo-larval stages: A case study with polystyrene (PS) and polymethylmethacrylate (PMMA) particles. *Environ. Res.* **2022**, *213*, 113584. [[CrossRef](#)] [[PubMed](#)]

Disclaimer/Publisher’s Note: The statements, opinions and data contained in all publications are solely those of the individual author(s) and contributor(s) and not of MDPI and/or the editor(s). MDPI and/or the editor(s) disclaim responsibility for any injury to people or property resulting from any ideas, methods, instructions or products referred to in the content.